






Article

# Carmeltazite, $ZrAl_2Ti_4O_{11}$ , a New Mineral Trapped in Corundum from Volcanic Rocks of Mt Carmel, Northern Israel

William L. Griffin <sup>1</sup>, Sarah E. M. Gain <sup>1,2</sup>, Luca Bindi <sup>3,\*</sup>, Vered Toledo <sup>4</sup>,  
Fernando Cámara <sup>5</sup>, Martin Saunders <sup>2</sup> and Suzanne Y. O'Reilly <sup>1</sup>

- <sup>1</sup> ARC Centre of Excellence for Core to Crust Fluid Systems (CCFS) and GEMOC, Earth and Planetary Sciences, Macquarie University, Sydney 2109, Australia; bill.griffin@mq.edu.au (W.L.G.); sarah.gain@mq.edu.au (S.E.M.G.); sue.oreilly@mq.edu.au (S.Y.O.)
- <sup>2</sup> Centre for Microscopy, Characterisation and Analysis, The University of Western Australia, Perth 6009, Australia; martin.saunders@uwa.edu.au
- <sup>3</sup> Dipartimento di Scienze della Terra, Università degli Studi di Firenze, Via G. La Pira 4, I-50121 Firenze, Italy
- <sup>4</sup> Shefa Yamim (A.T.M.) Ltd., Netanya 4210602, Israel; vered@shefayamim.com
- <sup>5</sup> Dipartimento di Scienze della Terra 'A. Desio', Università degli Studi di Milano, Via Luigi Mangiagalli 34, 20133 Milano, Italy; fernando.camara@unimi.it
- \* Correspondence: luca.bindi@unifi.it; Tel.: +39-055-275-7532

Received: 26 November 2018; Accepted: 17 December 2018; Published: 19 December 2018



**Abstract:** The new mineral species carmeltazite, ideally  $ZrAl_2Ti_4O_{11}$ , was discovered in pockets of trapped melt interstitial to, or included in, corundum xenocrysts from the Cretaceous Mt Carmel volcanics of northern Israel, associated with corundum, tistarite, anorthite, osbornite, an unnamed REE (Rare Earth Element) phase, in a Ca-Mg-Al-Si-O glass. In reflected light, carmeltazite is weakly to moderately bireflectant and weakly pleochroic from dark brown to dark green. Internal reflections are absent. Under crossed polars, the mineral is anisotropic, without characteristic rotation tints. Reflectance values for the four COM wavelengths ( $R_{min}$ ,  $R_{max}$  (%) ( $\lambda$  in nm)) are: 21.8, 22.9 (471.1); 21.0, 21.6 (548.3), 19.9, 20.7 (586.6); and 18.5, 19.8 (652.3). Electron microprobe analysis (average of eight spot analyses) gave, on the basis of 11 oxygen atoms per formula unit and assuming all Ti and Sc as trivalent, the chemical formula  $(Ti^{3+}_{3.60}Al_{1.89}Zr_{1.04}Mg_{0.24}Si_{0.13}Sc_{0.06}Ca_{0.05}Y_{0.02}Hf_{0.01})_{\Sigma=7.04}O_{11}$ . The simplified formula is  $ZrAl_2Ti_4O_{11}$ , which requires  $ZrO_2$  24.03,  $Al_2O_3$  19.88, and  $Ti_2O_3$  56.09, totaling 100.00 wt %. The main diffraction lines, corresponding to multiple  $hkl$  indices, are ( $d$  in Å (relative visual intensity)): 5.04 (65), 4.09 (60), 2.961 (100), 2.885 (40), and 2.047 (60). The crystal structure study revealed carmeltazite to be orthorhombic, space group  $Pnma$ , with unit-cell parameters  $a = 14.0951$  (9),  $b = 5.8123$  (4),  $c = 10.0848$  (7) Å,  $V = 826.2$  (1) Å<sup>3</sup>, and  $Z = 4$ . The crystal structure was refined to a final  $R_1 = 0.0216$  for 1165 observed reflections with  $F_o > 4\sigma(F_o)$ . Carmeltazite exhibits a structural arrangement similar to that observed in a defective spinel structure. The name carmeltazite derives from Mt Carmel ("CARMEL") and from the dominant metals present in the mineral, i.e., Titanium, Aluminum and Zirconium ("TAZ"). The mineral and its name have been approved by the IMA Commission on New Minerals, Nomenclature and Classification (2018-103).

**Keywords:** carmeltazite; Mt Carmel; volcanic rocks; corundum; spinel-derivative structure; desilication; extreme reduction

## 1. Introduction

During the study of the mineral assemblage of rock fragments recovered from volcanic tuffs and associated placer deposits in the drainage of the Kishon River, near Haifa (northern Israel), several

exotic phases have been identified as accessory minerals (e.g., [1] and references therein). In that area, a series of small volcanoes produced mafic to ultramafic pyroclastic rocks (vent breccias, tuffs) in upper Cretaceous time [2,3]. These rocks contain a wide variety of xenocrysts, including megacrysts of clinopyroxene, ilmenite, zircon and corundum. Among them, aggregates of corundum crystals (Carmel Sapphire™) are common in pyroclastic ejecta and in associated alluvial deposits. Many of these aggregates contain crystals of an unidentified Zr-Al-Ti-bearing phase, up to 80 µm in length. Chemical analysis and X-ray single-crystal diffraction studies allowed the characterization of the new Zr-Al-Ti phase, with the simplified formula  $ZrAl_2Ti_4O_{11}$ . This new mineral was named *carmeltazite* from Mt Carmel (“CARMEL”) and from the metals present in the mineral, i.e., Titanium, Aluminum and Zirconium (“TAZ”). The mineral and its name have been approved by the IMA Commission on New Minerals, Nomenclature and Classification, under the number 2018-103. The holotype specimen of *carmeltazite* is deposited in the mineralogical collections of the Museo di Storia Naturale, Università degli Studi di Firenze, Via G. La Pira 4, Florence, Italy, under catalogue number 3293/I.

The mineralogical description of *carmeltazite*, as well as its crystal structure, are given in this paper.

## 2. Occurrence of Carmeltazite

The new mineral described here, *carmeltazite*, occurs in pockets of trapped melt interstitial to, or included in, skeletal corundum crystals (Figures 1–3). The earliest parageneses consist of tistarite ( $Ti_2O_3$ ) ± *carmeltazite* ± Mg-Al spinel in a matrix of Ca-Mg-Al-Si-O glass.

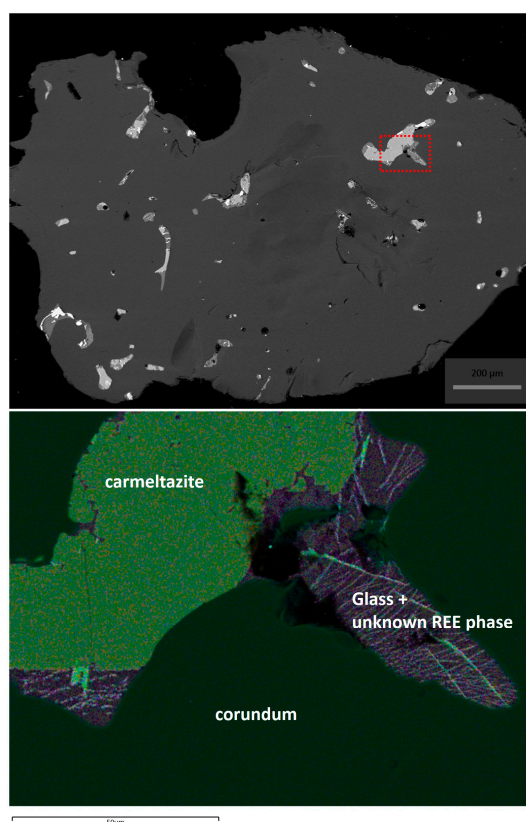


**Figure 1.** (Top) SEM-BSE image of *carmeltazite* (in corundum); scale bar is 200 µm; and (Bottom) phase map of the region highlighted in the top image with a red dashed rectangle (scale bar is 50 µm).

The silicate melts (probably basaltic) parental to this assemblage had previously been progressively desilicated by the exsolution of immiscible Fe-Ti oxide melts and Fe-Ti-Zr-silicide melts (found also as inclusions in *carmeltazite*; Figure 2), and the crystallization of moissanite and khamrabaevite (TiC),

at  $fO_2 = \Delta IW-6$  or less. This process continued, producing progressively lower  $fO_2$ , witnessed especially by the appearance of  $Ti^{2+}$ -bearing phases (osbornite, khamrabaevite, unnamed  $TiB_2$ , and unnamed  $TiO$ ).

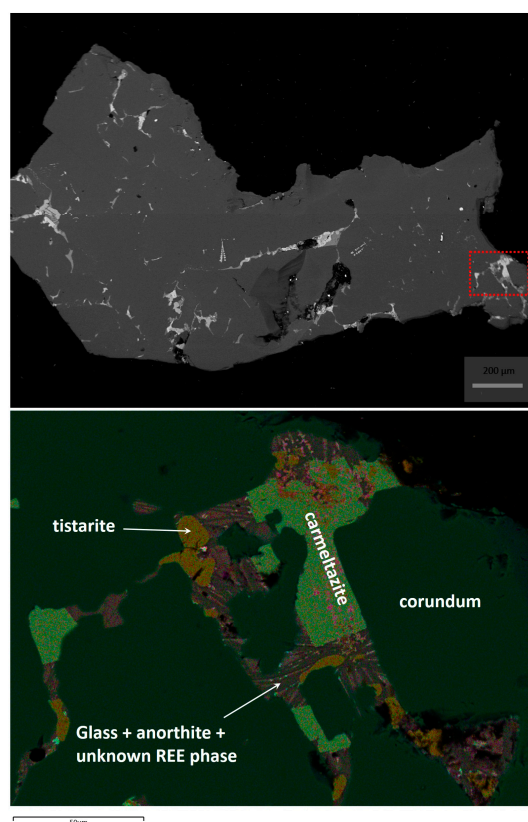


**Figure 2.** (Top) SEM-BSE image of carmeltaizite (in corundum); scale bar is 200 µm; and (Bottom) phase map of the region highlighted in the top image with a red dashed rectangle (scale bar is 50 µm).

### 3. Mineral Description and Physical Properties

Carmeltazite (Figure 1) occurs as black crystals, up to 80 µm in length and a few µm thick. The streak is reddish brown and the luster is metallic. The calculated density is  $4.122 \text{ g}\cdot\text{cm}^{-3}$  based on the ideal formula and single-crystal data (see below). Density was not measured because of the small amount of available material.

In plane-polarized incident light, carmeltaizite is weakly to moderately bireflectant and weakly pleochroic from dark brown to dark green. Internal reflections are absent. Under crossed polars, the mineral is anisotropic, without characteristic rotation tints.

The reflectance was measured in air by means of a MPM-200 microphotometer (CRAIC Technologies, San Dimas, CA, USA) equipped with a MSP-20 system processor on a Zeiss Axioplan ore microscope (Zeiss, Oberkochen, Germany). Filament temperature was approximately 3350 K. Readings were taken for specimen and standard (SiC) under the same focus conditions. The diameter of the circular measuring area was 0.05 mm. Reflectance percentages in the form ( $R_{\min}$ ,  $R_{\max}$  (%)) ( $\lambda$  in nm) are: 21.8, 22.9 (471.1); 21.0, 21.6 (548.3), 19.9, 20.7 (586.6); and 18.5, 19.8 (652.3).

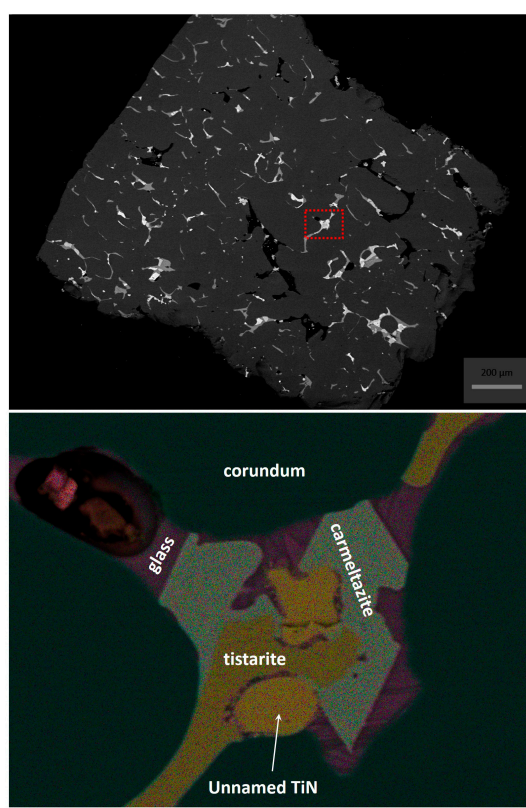


**Figure 3.** (Top) SEM-BSE image of carmeltaizite (in corundum); scale bar is 200  $\mu\text{m}$ ; and (Bottom) phase map of the region highlighted in the top image with a red dashed rectangle (scale bar is 25  $\mu\text{m}$ ).

#### 4. Chemical Data

Quantitative chemical analyses were carried out using a CAMECA-100X electron-microprobe (CAMECA Instruments, Gennevilliers, France), operating in WDS (Wavelength Dispersive Spectrometry) mode. The experimental conditions were: accelerating voltage 20 kV, beam current 20 nA, and beam size 1  $\mu\text{m}$ . Counting times are 15 s for peak and 20 s for background. Standards are (element, emission line): wollastonite (Si  $K\alpha$ , Ca  $K\alpha$ ), zircon (Zr  $K\alpha$ ), Hf wire (Hf  $L\alpha$ ), synthetic  $\text{UO}_2$  (U  $M\alpha$ ), synthetic  $\text{ThO}_2$  (Th  $L\alpha$ ), kyanite (Al  $K\alpha$ ), Cr metal (Cr  $K\alpha$ ), synthetic  $\text{TiO}_2$  (Ti  $K\alpha$ ), synthetic  $\text{ScPO}_4$  (Sc  $K\alpha$ ), synthetic  $\text{YPO}_4$  (Y  $K\alpha$ ), and synthetic MgO (Mg  $K\alpha$ ). Carmeltaizite is chemically homogeneous within the analytical uncertainties of our measurements. Table 1 gives analytical data (average of eight spot analyses).

**Table 1.** Chemical data of carmeltaizite.

Oxide	wt (%) ( $n = 8$ )	Range	Standard Deviation
$\text{SiO}_2$	1.50	1.24–1.70	0.24
$\text{ZrO}_2$	24.9	23.7–27.9	1.45
$\text{HfO}_2$	0.53	0.48–0.67	0.07
$\text{UO}_2$	0.16	0.00–0.40	0.15
$\text{ThO}_2$	0.06	0.00–0.13	0.05
$\text{Al}_2\text{O}_3$	18.8	18.0–20.1	0.78
$\text{Cr}_2\text{O}_3$	0.02	0.00–0.08	0.03
$\text{Ti}_2\text{O}_3$	50.6	48.8–52.2	1.30
$\text{Sc}_2\text{O}_3$	0.76	0.59–1.24	0.27
$\text{Y}_2\text{O}_3$	0.39	0.30–0.51	0.08
MgO	1.89	1.50–2.93	0.50
CaO	0.51	0.29–1.45	0.43
Total	100.12	98.87–100.5	0.28

The empirical formula (based on 11 oxygen atoms *pfu*, and assuming all Ti and Sc as trivalent) is  $(\text{Ti}^{3+}_{3.60}\text{Al}_{1.89}\text{Zr}_{1.04}\text{Mg}_{0.24}\text{Si}_{0.13}\text{Sc}_{0.06}\text{Ca}_{0.05}\text{Y}_{0.02}\text{Hf}_{0.01})_{\Sigma=7.04}\text{O}_{11}$ . The simplified formula is  $\text{ZrAl}_2\text{Ti}_4\text{O}_{11}$ , which requires  $\text{ZrO}_2$  24.03,  $\text{Al}_2\text{O}_3$  19.88, and  $\text{Ti}_2\text{O}_3$  56.09, totaling 100.00 wt %. The analytical total is excellent; the calculated relative error on the valence equilibrium  $Ev$  (defined as  $Ev(\%) = (Ev(+)-Ev(-)) \times 100/Ev(-)$ ) indicates a very small excess of positive charges.

## 5. X-ray Crystallography

A small carmeltazite fragment was extracted from the polished section shown in Figure 1 and mounted on a 5  $\mu\text{m}$  diameter carbon fiber, which was, in turn, attached to a glass rod. X-ray single-crystal intensity data were collected using an Oxford Diffraction Xcalibur 3 diffractometer (Oxford Diffraction Ltd., Abingdon, UK), equipped with a Sapphire 2 CCD area detector, with Mo  $K\alpha$  radiation. The detector to crystal working distance was 6 cm. The refined unit-cell parameters are:  $a = 14.0951$  (9),  $b = 5.8123$  (4),  $c = 10.0848$  (7)  $\text{\AA}$ , and  $V = 826.2$  (1)  $\text{\AA}^3$ .

The collected data were integrated and corrected for standard Lorentz polarization factors with the *CrysAlis* RED package [4]. The program ABSPACK in *CrysAlis* RED [4] was used for the absorption correction. In total, 1546 unique reflections were collected. The statistical tests ( $|E^2-1| = 0.980$ ) and the reflection conditions indicated the space group *Pnma*. The positions of most of the atoms were determined by means of direct methods. A least-squares refinement on  $F^2$  using heavy-atom positions and isotropic temperature factors gave an  $R$  factor of 0.156. Three-dimensional difference-Fourier synthesis yielded the position of the remaining atoms. The program *Shelxl-97* [5] was used for the refinement of the structure. Crystal data and details of the intensity data collection and refinement are reported in Table 2. We note here that the  $wR$  value is rather high, although we tried different absorption correction options.

**Table 2.** Crystal and experimental details for carmeltazite.

Crystal Data	
Crystal size ( $\text{mm}^3$ )	0.060 $\times$ 0.075 $\times$ 0.080
Cell setting, space group	Orthorhombic, <i>Pnma</i>
$a, b, c$ ( $\text{\AA}$ )	14.0951 (9), 5.8123 (4), 10.0848 (7)
$V$ ( $\text{\AA}^3$ )	826.2 (1)
Z	4
Data Collection and Refinement	
Radiation, wavelength ( $\text{\AA}$ )	Mo $K\alpha$ , $\lambda = 0.71073$
Temperature (K)	293
$2\theta_{\text{max}}$ ( $^\circ$ )	63.95
Measured reflections	12368
Unique reflections	1546
Reflections with $F_o > 4\sigma(F_o)$	1165
$R_{\text{int}}$	0.0134
$R\sigma$	0.0428
Range of $h, k, l$	$-20 \leq h \leq 20, -8 \leq k \leq 8, -15 \leq l \leq 15$
$R(F_o > 4\sigma(F_o))$	0.0216
$R$ (all data)	0.0242
$wR$ (on $F^2$ )	0.1426
Goof	0.911
Number of least-square parameters	103
Maximum and minimum residuals ( $e/\text{\AA}^3$ )	0.49 (at 1.53 from M1), $-0.51$ (at 1.02 from O4)

The site occupancy factor at the cation sites was allowed to vary (Ti vs. Al and Zr vs. Ti for the octahedral sites and Si vs. structural vacancy for the tetrahedral site) using scattering curves for neutral atoms taken from the *International Tables for Crystallography* [6].

The tetrahedral site showed a mean electron number of 12.6 and was thought to be occupied by Al and the available minor Si (i.e.,  $\text{Al}_{0.87}\text{Si}_{0.13}$ ). Indeed, although the site scattering was  $<13$  and the mean bond distance could indicate that minor Mg could substitute for Al, we thought that partitioning the minor Si in the tetrahedron would be the right choice. The M1 site, a site that shows a peculiar geometry with a 1 + 4 coordination with a refined site scattering of 14.3, was thought to be occupied by Al with minor Mg, Sc, Ca, Y and Hf (i.e.,  $\text{Al}_{0.68}\text{Mg}_{0.22}\text{Sc}_{0.04}\text{Ca}_{0.03}\text{Y}_{0.02}\text{Hf}_{0.01}$ ). The composition of M1 was refined simply as mixed Al + Ti site (see Supplementary Material: *carmeltazite.cif*). The mean electron numbers at the four octahedral M sites were the following: 37.3 (M2 site), 22.0 (M3 site), 20.7 (M4 site), and 20.8 (M5 site) corresponding to  $\text{Zr}_{0.85}\text{Ti}_{0.15}$ ,  $\text{Ti}_{1.00}$ ,  $\text{Ti}_{0.86}\text{Al}_{0.14}$ , and  $\text{Ti}_{0.87}\text{Al}_{0.13}$ , respectively. Altogether, taking into account the different multiplicity of the structural sites, the refined X-ray formula can be written as  $(\text{Ti}^{3+}_{3.75}\text{Al}_{1.94}\text{Zr}_{0.85}\text{Mg}_{0.22}\text{Si}_{0.14}\text{Sc}_{0.04}\text{Ca}_{0.03}\text{Y}_{0.02}\text{Hf}_{0.01})_{\Sigma=7.00}\text{O}_{11}$ . Such a formula is in excellent agreement with that obtained from electron microprobe:  $(\text{Ti}^{3+}_{3.60}\text{Al}_{1.89}\text{Zr}_{1.04}\text{Mg}_{0.24}\text{Si}_{0.13}\text{Sc}_{0.06}\text{Ca}_{0.05}\text{Y}_{0.02}\text{Hf}_{0.01})_{\Sigma=7.04}\text{O}_{11}$ .

Final atomic coordinates and equivalent isotropic displacement parameters are given in Table 3, whereas selected bond distances are presented in Table 4. Bond valence sums calculated using the parameters by Brese and O'Keeffe [7] and the following cation distributions are shown in Table 5:

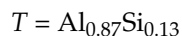
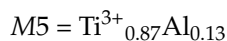
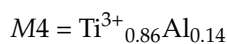
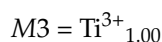
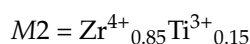
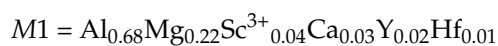


**Table 3.** Atom coordinates and equivalent isotropic displacement parameters ( $\text{\AA}^2$ ) for *carmeltazite*.

Atom	<i>x/a</i>	<i>y/b</i>	<i>z/c</i>	<i>U<sub>iso</sub></i>
M1	0.14578(9)	$\frac{1}{4}$	0.14765(13)	0.0400(4)
M2	0.00052(3)	$\frac{1}{4}$	0.77052(8)	0.0502(3)
M3	0.33102(5)	$\frac{1}{4}$	0.89039(8)	0.0374(3)
M4	0.33492(5)	$\frac{1}{4}$	0.42841(8)	0.0336(3)
M5	0.17178(4)	0.00094(10)	0.66151(5)	0.0356(2)
T	0.0406(1)	$\frac{1}{4}$	0.42210(15)	0.0435(5)
O1	0.0871(2)	$\frac{1}{4}$	0.5842(4)	0.0504(8)
O2	0.2458(2)	$\frac{1}{4}$	0.7435(3)	0.0478(9)
O3	0.2620(3)	$\frac{1}{4}$	0.2536(3)	0.0473(9)
O4	0.4168(2)	$\frac{1}{4}$	0.0695(3)	0.0412(7)
O5	0.4336(3)	$\frac{1}{4}$	0.5616(4)	0.0550(9)
O6	0.2446(3)	0.0018(3)	0.9994(2)	0.0485(8)
O7	0.4146(2)	0.0071(5)	0.3259(2)	0.0513(7)
O8	0.4141(2)	−0.0288(5)	0.8169(2)	0.0420(5)

**Table 4.** Selected bond distances (Å) for carmeltazite.

M1-O3	1.956(4)	M4-O5	1.933(4)
M1-O8	2.298(3) (×2)	M4-O6	1.978(3) (×2)
M1-O6	2.500(3) (×2)	M4-O3	2.041(4)
mean	2.310	M4-O7	2.079(3) (×2)
		mean	2.015
M2-O5	1.938(4)		
M2-O7	1.995(3) (×2)	M5-O3	1.965(2)
M2-O8	2.210(2) (×2)	M5-O2	1.966(2)
M2-O1	2.241(4)	M5-O6	2.015(3)
mean	2.098	M5-O1	2.031(3)
		M5-O7	2.057(2)
M3-O2	1.908(3)	M5-O4	2.132(2)
M3-O8	2.132(3) (×2)	mean	2.028
M3-O4	2.173(3)		
M3-O6	2.184(3) (×2)	T-O4	1.747(3)
mean	2.119	T-O1	1.761(4)
		T-O8	1.785(3) (×2)
		mean	1.770

**Table 5.** Bond valence calculations according to Brese and O’Keeffe [7].

Atom	M1	M2	M3	M4	M5	T	$\Sigma$ anions
O1	-	0.41	-	-	0.53 <sup>×2</sup>	0.69	2.16
O2	-	-	0.78	-	0.63 <sup>×2</sup>	-	2.04
O3	0.43	-	-	0.51	0.63 <sup>×2</sup>	-	2.20
O4	-	-	0.38	-	0.40 <sup>×2</sup>	0.71	1.89
O5	-	0.94	-	0.69	-	-	1.63
O6	0.10 <sup>×2</sup>	-	0.37 <sup>×2</sup>	0.61 <sup>×2</sup>	0.55	-	1.63
O7	-	0.80 <sup>×2</sup>	-	0.46 <sup>×2</sup>	0.49	-	1.75
O8	0.17 <sup>×2</sup>	0.45 <sup>×2</sup>	0.43 <sup>×2</sup>	-	-	0.65 <sup>×2</sup>	1.70
$\Sigma$ cations	0.97	3.85	2.76	3.34	3.23	2.70	-

Taking into account the refined mean electron numbers at the different sites, the cation-site preferences, and the polyhedral environments, we arrived to the site distributions reported above. Although we realize that some of the bond-valence sums (e.g., M1) are very far from the ideal values, we were not able to identify another site distribution that matches the refined site scattering values.

The diffraction rings (Table 6) from the same fragment used for the single-crystal study were obtained with an Oxford Diffraction Xcalibur PX Ultra diffractometer (Oxford Diffraction Ltd., Abingdon, UK) fitted with a 165 mm diagonal Onyx CCD detector (Oxford Diffraction, Abingdon, UK) and using copper radiation ( $\text{CuK}\alpha$ ,  $\lambda = 1.54138 \text{ \AA}$ ). The working conditions were: 50 kV, 50 mA, and 3 h of exposure; the detector-to-sample distance was 7 cm. The program *Crysalis RED* [4] was used to convert the observed diffraction rings to a conventional powder diffraction pattern. The least squares refinement gave the following values:  $a = 14.076 (2)$ ,  $b = 5.8124 (8)$ ,  $c = 10.0924 (9) \text{ \AA}$ , and  $V = 825.7 (1) \text{ \AA}^3$ .

**Table 6.** Calculated X-ray powder diffraction data for carmeltazite: 1 is the observed diffraction pattern, while 2 is the calculated diffraction pattern obtained with the atom coordinates reported in Table 3. Only reflections with  $I_{\text{calc}} > 10$  are listed. The five strongest reflections are given in bold.

<i>hkl</i>	1		2	
	$d_{\text{obs}}$	$I_{\text{est}}$	$d_{\text{calc}}$	$I_{\text{calc}}$
101	-	-	8.2017	31
201	5.78	20	5.7768	21
002			5.0424	35
011	<b>5.04</b>	<b>65</b>	5.0358	33
210	-	-	4.4841	17
202	-	-	4.1008	23
211	<b>4.09</b>	<b>60</b>	4.0973	56
212	-	-	3.3508	13
401	-	-	3.3266	11
410	-	-	3.0133	15
312	<b>2.961</b>	<b>100</b>	2.9587	100
013	-	-	2.9100	21
020	-	-	2.9062	17
411	<b>2.885</b>	<b>40</b>	2.8871	38
303	2.732	30	2.7339	32
213	-	-	2.6897	28
220	-	-	2.6867	18
221	2.597	20	2.5961	23
122	-	-	2.4787	18
413	-	-	2.2438	14
322	-	-	2.2193	14
421	-	-	2.1886	11
611	-	-	2.1289	10
404	2.051	25	2.0504	31
422	<b>2.047</b>	<b>60</b>	2.0486	54
504	-	-	1.8793	11
522	-	-	1.8779	16
332	-	-	1.6878	15
225	-	-	1.6130	12
722	-	-	1.5726	22
026	1.456	30	1.4550	25
040	-	-	1.4531	21
822	-	-	1.4436	18
1			3.9377	

## 6. Results and Discussion

### 6.1. Description of the Crystal Structure

The crystal structure of carmeltazite (Figure 4) is close to a defective spinel structure. The  $M_9O_{12}$  stoichiometry of a spinel becomes  $M_7O_{11}$  as one oxygen and two cations are lost. Nevertheless, the stacking of oxygen layers is not a cubic-close-packing yielding a standard ABCABC sequence along the cubic direction [111]. In carmeltazite, the sequence is hexagonal (the  $(hcc)_2$  of Tillmanns et al. [8]), i.e., ABACBC along [100]. Therefore, the two central layers are shifted and that changes the coordination of some atoms.



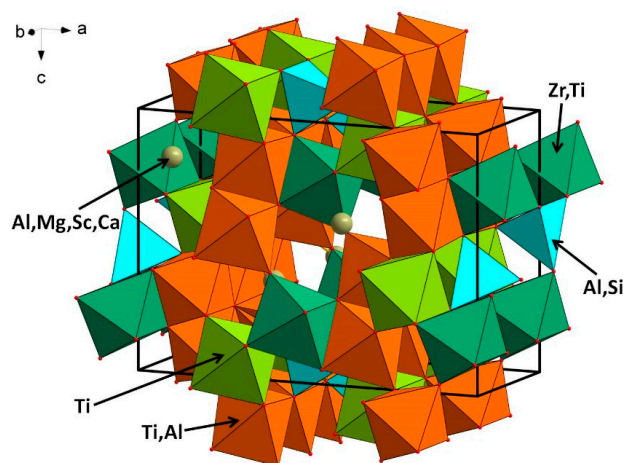


**Figure 4.** The crystal structure of carmelzite. The unit-cell and the orientation of the figure are outlined.

Figure 5 compares the stacking in carmelzite and spinel. The structural topology of carmelzite was already known for the synthetic compounds  $\text{Ba}_2\text{Ti}_{9,25}\text{Li}_3\text{O}_{22}$  [9],  $\text{SrLiCrTi}_4\text{O}_{11}$  and  $\text{SrLiFeTi}_4\text{O}_{11}$  [10], although, in those structures, the large alkaline-earth cation (Sr and Ba) substitutes for oxygen in the packing (the one which is missing in carmelzite), Li is in tetrahedral coordination (similar to Al in carmelzite) and  $\text{Ti}^{4+}$  and  $\text{Cr}^{3+}$  ( $\text{Fe}^{3+}$ ) are in octahedral coordination. The higher charge in M1 (Al) and M2 (Zr) in carmelzite allows for compensation of charge as Ti is only trivalent in carmelzite. However, the unusual coordination environment for the cations populating the M1 site in carmelzite (mostly Al and Mg) yields rather low bond valence sums (1.11 valence units). The Fourier-difference map was clean and therefore the presence of a partial occupation for the missing anion site is not supported by data. It is very probable that the location of the cation changes from one site to another, thus leading to a static disorder, although the shape of the displacement parameters is rather spherical. We also collected over-exposed frames (300 s) to search for possible diffuse scattering or weak satellite reflections (either incommensurate or commensurate with respect to the 3D unit cell chosen) to justify the odd M1 polyhedra (with very low valence sum) as due to the average nature of the structure, but no satellites were detected. Furthermore, the match between the powder diffraction pattern and that calculated from the structural model obtained here is further proof that the cation distribution cannot be far from the correct one.

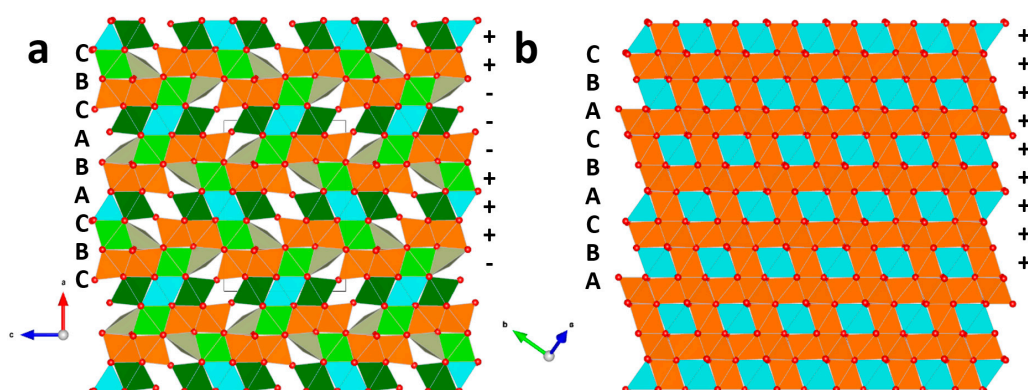


**Figure 5.** Comparison of the crystal structure of: carmelzite (a); and spinel (b). Observe the alternation of the layers, promoting the presence of vacant sites and pyramidal coordination for the M1 site in carmelzite.

## 6.2. Origin of Carmeltazite

The corundum aggregates in which the carmeltazite occurs appear to have formed near the crust-mantle boundary (ca. 30 km depth [11]), in the presence of excess volatiles. The abundance of carbon in the system (SiC, TiC and amorphous C as common phases) and the low  $fO_2$  required by the observed assemblages ( $\Delta IW$   $-6$  to  $-10$  [12]) suggests that the volatiles were dominated by mantle-derived  $CH_4 + H_2$ , which reduced a volume of mafic to ultramafic melt. The unusual conditions have resulted in many previously unknown phases, which are the subject of ongoing investigations.

## 7. Conclusions

The mineralogical assemblage at Mt Carmel shows several analogies with those observed in calcium-aluminum inclusions (CAIs) in carbonaceous chondrites (CCs). Besides the recently described tistarite [2], hibonite [11] and krotite [1], the new mineral described here resembles the Zr-bearing phases found in CC, e.g., panguite [13], kangite [14] and allendeite [15]. Furthermore, although the inferred conditions of the Mt Carmel assemblages are similar to those of the CAIs in terms of temperature and  $fO_2$ , crystallization appears to have formed at higher pressures, ca. 1 GPa. These analogies suggest that the Mt Carmel system also formed in presence of abundant  $H_2$  and carbon. Such a hypothesis recently has been verified by the discovery of the first natural hydride in the same Israeli volcanic xenocrysts [12].

**Supplementary Materials:** The following are available online at <http://www.mdpi.com/2075-163X/8/12/601/s1>, carmeltazite.cif.

**Author Contributions:** W.L.G., S.E.M.G., V.T., M.S. and S.Y.O. found the new mineral and carried out the electron microprobe analyses; L.B. performed the X-ray single-crystal experiments; L.B. and F.C. analyzed the data; and L.B. wrote the paper with input from all coauthors.

**Acknowledgments:** The research was supported by “progetto d’Ateneo 2016, University of Firenze” to Luca Bindi, from the ARC Centre of Excellence for Core to Crust Fluid Systems (<http://www.cafs.mq.edu.au>), contributions 1229, and contribution 1269 from the GEMOC Key Centre (<http://www.gemoc.mq.edu.au>). The authors also acknowledge the facilities, and the scientific and technical assistance of Microscopy Australia at the Centre for Microscopy, Characterisation & Analysis, The University of Western Australia, a facility funded by the University, State and Commonwealth Governments.

**Conflicts of Interest:** The authors declare no conflict of interest.

## References

1. Griffin, W.L.; Gain, S.E.M.; Huang, J.-X.; Saunders, M.; Shaw, J.; Toledo, V.; O’Reilly, S.Y. A terrestrial magmatic hibonite-grossite-vanadium assemblage: Desilication and extreme reduction in a volcanic plumbing system, Mt Carmel, Israel. *Am. Miner.* **2019**. [CrossRef]
2. Griffin, W.L.; Gain, S.E.M.; Adams, D.T.; Huang, J.-X.; Saunders, M.; Toledo, V.; Pearson, N.J.; O’Reilly, S.Y. First terrestrial occurrence of tistarite ( $Ti_2O_3$ ): Ultra-low oxygen fugacity in the upper mantle beneath Mount Carmel, Israel. *Geology* **2016**, *44*, 815–818. [CrossRef]
3. Xiong, Q.; Griffin, W.L.; Huang, J.-X.; Gain, S.E.M.; Toledo, V.; Pearson, N.J.; O’Reilly, S.Y. Super-reduced mineral assemblages in “ophiolitic” chromitites and peridotites: The view from Mount Carmel. *Eur. J. Mineral.* **2017**, *29*, 557–570. [CrossRef]
4. Oxford Diffraction. *CrysAlis RED (Version 1.171.31.2) and ABSPACK in CrysAlis RED*; Oxford Diffraction Ltd.: Abingdon, Oxfordshire, UK, 2006.
5. Sheldrick, G.M. A short history of SHELX. *Acta Cryst.* **2008**, *A64*, 112–122. [CrossRef] [PubMed]
6. Wilson, A.J.C. *International Tables for Crystallography. Volume C: Mathematical, Physical and Chemical Tables*; Kluwer Academic: Dordrecht, The Netherlands, 1992.
7. Brese, N.E.; O’Keeffe, M. Bond-valence parameters for solids. *Acta Cryst.* **1991**, *B47*, 192–197. [CrossRef]
8. Tillmanns, E.; Hofmeister, W.; Baur, W.H. Variations on the theme of closest packing: The structural chemistry of barium titanate compounds. *J. Solid State Chem.* **1985**, *58*, 14–28. [CrossRef]
9. Tillmanns, E.; Wendt, I. Die Kristallstruktur eines Bariumtitanlithiumoxids,  $Ba_2Ti_{9,25}Li_3O_{22}$ . *Zeit. Kristallogr.* **1976**, *144*, 16–31. [CrossRef]

10. Imaz, I.; Péchev, S.; Koseva, I.; Bourée, F.; Gravereau, P.; Peshev, P.; Chaminade, J.-P. Structural filiations in the new complex titanates  $\text{SrLiMTi}_4\text{O}_{11}$  ( $M = \text{Cr, Fe}$ ). *Acta Cryst.* **2007**, *B63*, 26–36. [[CrossRef](#)] [[PubMed](#)]
11. Griffin, W.L.; Huang, J.-X.; Thomassot, E.; Gain, S.E.M.; Toledo, V.; O'Reilly, S.Y. Super-reducing conditions in ancient and modern volcanic systems: Sources and behaviour of carbon-rich fluids in the lithospheric mantle. *Min. Petr.* **2018**, *112*, 1–14. [[CrossRef](#)]
12. Bindi, L.; Cámara, F.; Griffin, W.L.; Huang, J.-X.; Gain, S.E.M.; Toledo, V.; O'Reilly, S. Solar nebula conditions on Earth produced the first natural hydride. *Sci. Rep.* **2019**. submitted.
13. Ma, C.; Tschauner, O.; Beckett, J.R.; Rossman, G.R.; Liu, W. Panguite,  $(\text{Ti}^{4+}, \text{Sc, Al, Mg, Zr, Ca})_{1.8}\text{O}_3$ , a new ultra-refractory titania mineral from the Allende meteorite: Synchrotron micro-diffraction and EBSD. *Am. Mineral.* **2012**, *97*, 1219–1225. [[CrossRef](#)]
14. Ma, C.; Tschauner, O.; Beckett, J.R.; Rossman, G.R.; Liu, W. Kangite,  $(\text{Sc, Ti, Al, Zr, Mg, Ca, } \square)_2\text{O}_3$ , a new ultra-refractory scandian mineral from the Allende meteorite: Synchrotron micro-Laue diffraction and electron backscatter diffraction. *Am. Mineral.* **2013**, *98*, 870–878. [[CrossRef](#)]
15. Ma, C.; Beckett, J.R.; Rossman, G.R. Allendeite ( $\text{Sc}_4\text{Zr}_3\text{O}_{12}$ ) and hexamolybdenum ( $\text{Mo, Ru, Fe}$ ), two new minerals from an ultrarefractory inclusion from the Allende meteorite. *Am. Mineral.* **2015**, *99*, 654–666. [[CrossRef](#)]



© 2018 by the authors. Licensee MDPI, Basel, Switzerland. This article is an open access article distributed under the terms and conditions of the Creative Commons Attribution (CC BY) license (<http://creativecommons.org/licenses/by/4.0/>).